# Fundamental Mechanisms of Phosphate Stabilization of Divalent Metals in MSW Combustion Scrubber Residues

T. Taylor Eighmy
Environmental Research Group
A115 Kingsbury Hall
University of New Hampshire
Durham, NH 03824

Bradley J. Crannell
Environmental Research Group
A115 Kingsbury Hall
University of New Hampshire
Durham, NH 03824

Leslie G. Butler
Chemistry Department
Louisiana State University
Baton Rouge, LA 70803

Frank K. Cartledge
Chemistry Department
Louisiana State University
Baton Rouge, LA 70803

Earl Emery
Chemistry Department
Louisiana State University
Baton Rouge, LA 70803

Daniel Oblas
Center for Advanced Materials
University of Massachusetts Lowell
1 University Avenue
Lowell, MA 01854

James E. Krzanowski
Mechanical Engineering Department
134 Kingsbury Hall
University of New Hampshire
Durham, NH 03824

J. Dykstra Eusden Jr.
Geology Department
Carnegie Hall
Bates College
Lewiston, ME 04240

Elizabeth L. Shaw
Analytical Shared Experimental Facility
Center for Material Science and Engineering
Room 13-4137
Massachusetts Institute of Technology
77 Massachusetts Avenue
Cambridge, MA 02139

Carl A. Francis
Harvard University Mineralogical Museum
24 Oxford Street
Cambridge, MA 02138

## INTRODUCTION

Chemical stabilization of waste materials offers the potential to reduce the leachability of heavy metals in the waste. The principal objective during stabilization is to form new mineral phases with reduced solubilities and increased geochemical stability in a leaching environment. One stabilization agent of recent interest, particularly for $Pb^{2+}$, is $PO_4^{3-}$.[1,2,3,4,5]

A patented soluble phosphate treatment process, marketed by Wheelabrator Environmental Systems as the WES-PHix process, is used in 23 MSW combustion or ash processing facilities in the United States. It is also used at 7 wire recycling facilities. The process is licensed to Kurita Water Industries Ltd. of Japan where it is marketed as the ASHNITE process. It is used in over 80 MSW combustion or ash processing facilities in Japan.

Phosphate combines with over 30 elements to form about 300 naturally-occurring minerals.[6,7] Metal phosphates are ubiquitous secondary minerals in the oxidized zones of lead ore deposits and as assemblages around ore bodies.[7] They also occur in soils, sediments, and phosphatic beds.[7] As such, they are stable with respect to pH, Eh, and mineral diagenesis. Isomorphic substitutions are very common for both divalent cations (e.g. $Pb^{2+}$ for $Ca^{2+}$) and oxyanions (e.g. $AsO_4^{3-}$ for $PO_4^{3-}$) in these minerals.[7]

Past research efforts have shown that phosphate minerals are likely controlling solids for $Ca^{2+}$, $Cd^{2+}$, $Cu^{2+}$, $Pb^{2+}$ and $Zn^{2+}$ in natural soil systems.[8,9,10,11,12,13] The use of $PO_4^{3-}$ to immobilize metals has been advocated for industrial wastewaters[14,15] and lead-contaminated soils.[13,16,17,18,19,20] Both phosphate-containing minerals and soluble phosphate have been advocated as sources of $PO_4^{3-}$.

In the case of phosphate-containing minerals as a $PO_4^{3-}$ source, the ongoing work by Traina's group[4,16,17,18,19,20] has explored apatites (e.g. calcium hydroxyapatite, $Ca_5(PO_4)_3OH$) or waste phosphate rock as a source of $PO_4^{3-}$ to precipitate $Pb^{2+}$ from solution or in contaminated soils as lead hydroxypyromorphite ($Pb_5(PO_4)_3OH$); a more thermodynamically stable isostructural analogue to calcium hydroxyapatite.[4]

In the case of soluble phosphate as a $PO_4^{3-}$ source, chemical stabilization mechanisms can involve a continuum from surface sorption processes to existing or newly formed particulate surfaces in a waste material, through the formation of new surface precipitates, to the formation of discrete heterogeneous or homogeneous precipitates.[21] Spectroscopic and geochemical modeling techniques exist to help distinguish between sorption and the various forms of precipitation (e.g. surface, heterogeneous, homogeneous).[22,23,24,25]

When soluble phosphate is used to stabilize metals in waste materials containing appreciable concentrations of $Ca^{2+}$, it is useful to understand $Ca^{2+}$ and $PO_4^{3-}$ crystallization and precipitation chemistry as this reaction sequence is likely to dominate the system. When $Ca^{2+}$ and $PO_4^{3-}$ are titrated in solution, a variety of phases form.[26,27] In a simple system, the reaction sequence generally involves $Ca_9(PO_4)_6$ (non-stoichiometric amorphous calcium phosphate), $CaHPO_4 \cdot 2H_2O$ (brushite); $CaHPO_4$ (monetite); $Ca_8H_2(PO_4)_6 \cdot 5H_2O$ (octacalcium phosphate), $\beta$-$Ca_3(PO_4)_2$ (whitlockite); and ultimately $Ca_5(PO_4)_3OH$ (calcium hydroxyapatite); the most geochemically stable calcium phosphate.[28] The sequence is influenced by ion activity products (IAPs), pH, ionic strength, reaction kinetics, the presence of precursor substrates or "seed", and the presence of inhibitors like $Mg^{2+}$.[26,27,29]

This reaction sequence is useful in interpreting likely immobilization mechanisms in $Ca^{2+}$- containing waste materials treated with $PO_4^{3-}$. There is evidence for relatively fast sorption processes onto calcium hydroxyapatite at low metals concentration for $Cd^{2+}$, $Cu^{2+}$, $Pb^{2+}$, and $Zn^{2+}$.[15,30,31,32] At higher metals concentration, evidence of surface precipitation on the calcium hydroxyapatite is observed; more so for $Pb^{2+}$ and less so for $Cd^{2+}$ and $Zn^{2+}$.[5,33] In systems where $Pb^{2+}$ is present in high concentrations in solution, evidence is given that less stable calcium hydroxyapatite will dissolve and preprecipitate as more stable lead hydroxypyromorphite.[4,5,16,17,18,19,20] In systems where all components are initially soluble, it is simple to precipitate lead hydroxypyromorphite[7,10] or ternary metal apatites where $Pb^{2+}$, $Cd^{2+}$, $Cu^{2+}$, and $Zn^{2+}$ isostructurally substitute for $Ca^{2+}$ and form solid solutions like $(Ca, Pb, Zn)_5(PO_4)_3OH$.[34,35]

Dry scrubber residue is a particulate material from the use of dry lime powder (CaO) or dried slaked lime powder ($Ca(OH)_2$) in the scrubbing of flue gas from combustion of municipal solid waste. This is the second largest residual stream for modern waste to energy facilities.[36] The residue contains high concentrations of acid gas scrubber products (e.g. $CaCl_2$, $CaSO_4$), unreacted scrubber material (CaO or $Ca(OH)_2$), condensed semivolatile elements (e.g. $Cl^-$, $Pb^{2+}$), condensed volatile elements (e.g. $Na^+$, $K^+$, $Hg^{2+}$, $Zn^{2+}$ and $Cd^{2+}$), aluminosilicate fly ash particles, and char.[37] The fine-grained residue is highly soluble and very alkaline, making it sometimes difficult to treat or dispose.[36]

The approach taken by our group to understand stabilization mechanisms and identify reaction products formed during treatment of scrubber residues is shown in Figure 1. A variety of spectroscopic and geochemical modeling procedures are used as each provides specific and complementary information and because some suffer from small databases relative to the more exotic mineral phases found in granular waste materials.

This study was designed to determine the mechanisms and reaction products of chemical stabilization of dry scrubber residues treated with soluble orthophosphate. The data gleaned from various spectroscopic analyses, leaching procedures, and geochemical modeling show that precipitation/solid solution formation rather than sorption is the immobilization mechanism and that apatite minerals and solid solutions are the principal solubility-controlling reaction products. As in nature, these minerals are geochemically stable and very insoluble.

These results hold promise for the industry. Knowledge about the basic mechanisms of immobilization allows for further optimization of the process. Successful identification of reaction products using both spectroscopic and geochemical modeling techniques provides confidence for the use of geochemical models as predictive tools for refining treatment formulations, examining long term disposal behavior, and developing management strategies. Research is also ongoing by our group on soluble phosphate treatment mechanisms in MSW bottom ash, MSW ash vitrification dusts, smelter dusts, electric arc furnace dusts, and mine tailings.

## METHODS

### Combustor Description

A 1,500 ton per day mass burn facility was sampled. It consists of two parallel units comprised of reciprocating grates, water wall boilers, scrubber venturis, and $Ca(OH)_2$ scrubbers with fabric filters. Activated carbon is used as a mercury sorbent; it is injected with the lime. It was operational during sampling.

Sampling occurred over the period from January 3rd to January 7th, 1995. Dry scrubber residue was collected by plant personnel. A grab sample (1 kg) was collected every 10 minutes to make a 4 hour daily composite from one of the scrubber transfer conveyors. The five daily composites were made into a weekly composite using a clean, lab-scale cement mixer.

**Processing**

For the purposes of this study, an experimental laboratory-scale treatment formulation was selected to ensure that stabilization reaction mechanisms and reaction products could be detected. A standard industrial grade $H_3PO_4$ acid solution was used. The treatment formulation involved using a dose of 1.2 moles $H_3PO_4$ per kg of residue. Process mixing water at a liquid to solid (L/S) ratio of 0.4 was used to facilitate mixing. The residues were mixed for 10 minutes in a Hobart mixer and then air dried. The mixing regime is similar to full scale treatment systems. The treated working sample was subsampled for subsequent analyses; the subsample was stored under vacuum desiccation until use.

**Total Composition**

The dry scrubber residues were quantified for over 47 elements using neutron activation analysis (NAA) for all elements except Pb, Cu, P, S, C and O. Procedures are provided elsewhere.[38,39,40] X-ray fluorescence (XRF) was used for Pb, Cu, S, and P analyses. X-ray photoelectron spectroscopy (XPS) was used to quantify C and O (see below).

**STEM-XRM**

STEM-XRM was used to examine discrete particle morphology and determine elemental composition and possible mineral formula in discrete particles of the treated and unleached as well as the treated and leached fractions. STEM examinations were conducted on a Hitachi H-600 TEM operated at 100 kV accelerating voltage.

**SIMS**

SIMS was used to elucidate the stabilization mechanism. The method was used to depth profile selected atomic masses ($^{40}Ca^+$, $^{208}Pb^+$, $^{31}P^+$, $^{35}Cl^+$, $^{28}Si^+$) so as to examine concentration as a function of particle depth (particle exterior to interior). This would provide evidence of possible surface adsorption or surface precipitation or evidence of new discrete phase precipitation.[24]

A Fisons/VG SIMSLAB I (upgraded) quadrapole filter type mass analyzer was used to conduct positive ion (+m/z) depth profiling using an $O_2^+$ ion beam source. Profiles were conducted at high vacuum ($10^{-9}$ torr). Indium foil was used for sample mounting to minimize charging. Generally, the ion source was operated at 10 keV and 20 nA. Target biases were usually 5-15V. The profiles were done at 200x with the extractor operated at 1,500 V. Estimated sputtering rates were roughly 1 to 10 Å per second. Profiles for $^{208}Pb^+$, $^{31}P^+$, $^{40}Ca^+$, $^{28}Si^+$, $^{35}Cl^+$, and $^{113}In^+$ were usually conducted for 45 minutes to 1 hour.

**XRPD**

XRPD was used to identify crystalline mineral phases in the residues. A Rigaku-Geigerflex goniometer was used along with a copper X-ray source (45 kV, 35 mA, 1500 W). A divergence slit of 1°, a scattering slit of 1°, a receiving slit (crystal) of 0.8°, and a receiving slit (monochromator) of 0.6° were used. Details on search-match procedures are provided elsewhere[38].

**MAS-NMR**

MAS NMR was used to monitor the $^{31}P$ isotropic chemical shifts and chemical shift anisotropy tensors of the component species in the treated and unleached as well as the treated and leached fractions. The

spectra were taken on a 400 MHz Chemagnetics Infinity NMR spectrometer with a 9.4 Tesla magnet corresponding to a $^{31}P$ NMR frequency of 161.9 MHz. The samples were spun in 7.5 mm (OD) zirconia rotors in a double resonance probe at spin rates between 1 to 7 kHz at a temperature of about 23 ± 2 °C. The magic angle was set by observing the chemical shift of the aromatic resonance of hexamethylbenzene. The spin rate was measured with a fiberoptic sensor and is accurate to ±2 Hz. All spectra were recorded with proton decoupling while using 10 μs 90° $^{31}P$ pulses (except where noted); pulse lengths were calibrated by observing the $^{31}P$ resonance of $NH_4H_2PO_4$ (ammonium dihydrogen phosphate). The recycle delay was set to 10 s based on approximate $^{31}P$ $T_1$ measurements of some of the samples. The number of scans acquired ranged from 500 to 4,000. Chemical shifts were referenced to an external standard sample of $NH_4H_2PO_4$.; ($\delta$ ($^{31}P$) = 0 ppm with respect to 85% $H_3PO_4$.[41]

The analysis of $^{31}P$ NMR spectra of inorganic phosphates is generally done by a consideration of both the isotropic chemical shift and the individual chemical shift tensor elements (principal axis system). These values are obtained from the $^{31}P$ NMR spectrum using the graphical method of Herzfeld and Berger[42] or by a Simplex and gradient search method.[43] The latter was used here as it is optimized for multiple component systems.

**XPS**

A Perkin Elmer Physical Electronics Division 5100 hybrid XPS was used to identify and quantify possible chemical phases as well as to quantify elements in the samples. Detailed methods are provided elsewhere.[38] For energy referencing, the entire system was calibrated to the gold 84.0 $4f_{7/2}$ binding energy. Correction for peak shift due to static charge buildup on the sample was achieved through the adventitious carbon reference method using a C 1s binding energy of 284.8 eV as a conducting reference.[44] Details on full width, half maximum values used for curve fitting[45, 46,47] as well as spectral deconvolution are provided elsewhere[38].

**Leaching Apparatus**

All leaching tests were conducted in leaching apparatus maintained in a laminar flow hood (Envirco, Houston, Texas) with Type 2 HEPA air filters (>0.3 μm). The apparatus is comprised of parallel units; each consisting of a 1000 ml Teflon leaching vessel with a screw cap, a stir plate, a stir bar, and constant temperature bath (25°C). Each vessel was maintained at a constant pH using a Cole-Parmer pH/ORP Controller (Model 5652-10). The controller opens and closes solenoids allowing the introduction of strong acid (3N $HNO_3$) or base (3N NaOH). The set points on the controller allowed for a ±0.1 pH variation around a target value.

**Total Availability Leaching Procedure**

The procedure is based on the Dutch Total Availability Leaching test NEN 7341.[48] It was used to quantify the elemental mass fraction available for leaching. The method can assess what fraction of the total concentration of an element is leachable over geologic time (1,000-10,000 years). During the extraction, all readily soluble and marginally soluble minerals will solubilize. Desorption of tightly sorbed species will also occur. Details are provided elsewhere[38].

After filtration the leachates were combined. The sample was then split for metals analysis (graphite furnace and flame atomic absorption spectrophotometry,), anions analysis (ion chromatography), and alkalinity determinations (titration).[49,50,51] Additionally, the weight of the leached residue was determined for mass balance purposes. Residues were dried for 72 hours at 60°C to obtain a dry weight measure.

### pH-Dependent Leaching

The pH-dependent leaching procedure is a means of determining the equilibrium leaching behavior over a range of pH values. Each extraction was done at a L/S ratio of 10.0 so as to ensure solid phase control. Eighty grams of sample were placed into the Teflon vessel to which 800 mls of distilled, deionized water was added. 3N $HNO_3$ was used to control the pH at various set points 4,6,8 for 24 hours. This pH range corresponds to values expected for both regulatory leaching tests and open $CO_2(g)$ leaching systems (e.g. landfills). The leachates were filtered and analyzed as described above. Additionally, $Pb^{2+}$ was determined using isotope dilution procedures and thermal ionization mass spectrometry after ion exchange concentration.[52] $PO_4^{3-}$ was also determined by using a Lachat low level colorimetric assay.[53]

### Leaching Modeling

The geochemical equilibrium model MINTEQA2[54] was used to determine which solid phase controlled leachate composition as a function of pH. The thermo.dbs and type6.dbs databases for MINTEQA2 were modified to include a large number of phosphate mineral phases shown in Table 1. Modeling details are provided elsewhere[38].

The likelihood of solid solution formation during dissolution and reprecipitation required further modification to the MINTEQA2 databases to allow for idealized solid solutions to act as possible controlling solids. A simplistic zero heat of mixing and ideal site substitution model was assumed.[59,60] Standard free energies of formation for the solid solutions ($\Delta G^o_{f,ij}$) between end members i and j were used to determine theoretical $K_{sp}$ values for the solid solutions using:

$$\Delta G^o_{f,ij} = x\Delta G^o_{f,i} + (1-x)\Delta G^o_{f,j} + nRT\,[x \ln x + (1-x) \ln (1-x)] \quad (1)$$

where x is the mole fraction of end member i, $\Delta G^o_{f,i}$ and $\Delta G^o_{f,j}$ are the free energies of formation of end members i and j, respectively, n is the number of sites in the mineral undergoing substitution (e.g. 1.0), R is the universal gas constant, and T is degrees Kelvin. $K_{sp}$ values for hypothetical binary ideal solid solutions [e.g. for (Ca,Pb), (Ca,Cu), (Ca, Cd), and (Ca, Zn)] for the minerals $Ca_3(PO_4)_2$, $Ca_5(PO_4)_3OH$, $Ca_5(PO_4)_3Cl$, and $Ca_4O(PO_4)_2$ (Pb and Ca only) were calculated and entered into the MINTEQA2 databases. No attempts were made to evaluate the likelihood of these solid solutions with respect to theoretical (e.g. $K_{sp,i}/K_{sp,j}$) or experimental distribution coefficients.

## RESULTS AND DISCUSSION

### Total Composition

Table 2 provides information on the total elemental composition of the dry scrubber fabric filter residue as determined by NAA, XRF, and XPS. The major constituents (> 10,000 mg/kg) in the fabric filter residue were O, Ca, Cl, C, Si, Al, S, Na, and Zn. Minor constituents (1,000-10,000 mg/kg) included K, Ti, Fe, Mg, Pb, and Br. Trace constituents (< 1,000 mg/kg) included Cd, Cr, Hg, and many other elements. These concentrations are fairly typical for MSW dry scrubber fabric filter residues.[36] The presence of small quantities of activated carbon as a mercury sorbent may explain the relatively high C concentrations as well as the relatively high Hg concentrations in the residues. The concentrations of S, Pb, Cd, Cu, and Zn are in typical ranges for these wastes.[36] The observed phosphorus concentration, 2,100 mg/kg, is within the range of reported values (1,700 to 4,600 mg/kg) for untreated scrubber residues.

**Particle Composition Based on STEM-XRM**

Table 3 contains the atomic percent data generated from the analysis of discrete particle assemblages with STEM-XRM. Analyses were conducted on 10 assemblages for both the treated unleached and the treated and leached fractions. Particles were polycrystalline and small (100-5,000 nm). A wide variety of elements were observed in the residues. For the treated and unleached residues, O, Ca and Cl were very common elements. Mg, Al, Si, P, S, and K were also present. No Fe, Zn or Pb was observed. For the treated and leached residues, O, Al, P, S, Ca, Fe and Zn were very common elements. Mg, Si, Cl and K were also observed. Leaching appeared to have increased the relative concentration of many elements, particularly Al, P, Fe and Zn. This occurred because of the relative loss of Cl, K and Ca.

It is very likely that given the very small particle sizes that were interrogated (100 to 5,000 nm) as well as the complex structure of the polycrystalline particles, discrete homogeneous single crystals were not analyzed. The determination of molecular formulas from the data proved tedious and inconclusive.

It is important to note that the elements that were observed are many of the major and minor elements seen in the residues with total compositional analyses. Further, the elemental complexities of the assemblages agrees in principal with the types of phases observed with other methods like XRPD and XPS (see below). Finally, virtually all of the assemblages contained phosphorus; particularly in the leached residues. This is viewed favorably with respect to the availability of the stabilization agent to all particles at the nanometer scale under the mixing regime that was used.

**Stabilization Reaction Mechanism Based on SIMS**

Figure 2a shows typical depth profiles for the mineral standard $Ca_5(PO_4)_3Cl$ (calcium chloroapatite; Harvard University Mineralogical Museum 107354) which was ground to very small particle sizes (<50 μm). This control sample represents a "homogeneous precipitate". As can be seen in the figure, $^{40}Ca^+$, $^{31}P^+$ and $^{35}Cl^+$ were relatively constant with depth (up to depth less than or equal to 0.5 μm). The background indium foil signal is also relatively constant. As expected, the homogeneous particulate gave a rather uniform depth profile for all of its constituents.

Figure 2b shows typical depth profiles for the treated and unleached fraction (other fraction mass fragment depth profiles are not shown). The profiles are similar to the calcium chloroapatite standard. Elements were uniformly distributed with depth. More $^{31}P^+$ was present in the treated residue than in the chloroapatite. The $^{113}I^+$ and $^{28}Si^+$ profiles did not change significantly with depth (up to less than or equal to 0.5 μm).

The use of ion mass fragment ratios is more illustrative of relative behaviors as a function of depth. $^{40}Ca^+$ is used to normalize the data. As shown in Figure 2c, the $^{31}P^+/^{40}Ca^+$ ratios in the chloroapatite, treated and unleached fraction and the untreated and unleached fraction were similar. The $^{31}P^+/^{40}Ca^+$ ratio was relatively constant with depth. These ratio profiles are similar to ones reported by Fulghum et al.[24] for the coprecipitate. They differ markedly from the adsorbed scenario. This suggests that the stabilization process produced a homogeneous precipitate. Stabilization via surface sorption was not likely. The leached residues showed clear enrichment of P relative to Ca in the particle surface. This is ascribed to preferential loss of Ca and salts during leaching at pH 4.0 in the Total Availability Leaching test. Though resorption of $PO_4^{3-}$ cannot be ruled out at pH 4.0, the other spectroscopic techniques (particularly XPS) also showed clear loss of calcium in the outer particle surfaces during leaching.

The $^{208}Pb^+/^{40}Ca^+$ ratios showed similar, though less dramatic behavior, to the $^{31}P^+/^{40}Ca^+$ ratios as a function of depth. As shown in Figure 2d, the leached samples were surface enriched in $^{208}Pb^+$ while the

unleached samples showed uniform distribution as a function of depth. Contrary to $PO_4^{3-}$ resorption, $Pb^{2+}$ will not readily sorb at pH 4 so the data support the theory that the surface enrichment is an artifact of Ca salt loss during leaching. Similar behaviors were seen with the untreated and leached residues, though heterogenaity at the nm level was less than heterogenaity with depth.

These results strongly suggest that stabilization of $Ca^{2+}$ and $Pb^{2+}$ is largely via $PO_4^{3-}$- based precipitation and not by surface sorption processes. The former reaction mechanism is more geochemically stable and resistant to leaching than the later mechanism. However, it is also likely that at a smaller spatial scale level, some sorption processes are occurring. There are other techniques that can be employed to verify the presence or absence of sorption processes.[22,25] However, sorption isotherms, desorption assays, and isotopic exchange experiments are problematic with respect to the highly soluble nature of these residues. The use of SIMS is just one spectroscopic technique that was used in elucidating reaction mechanisms.

**Phosphate Crystalline Phase Identification Based on XRPD**

Table 4 contains possible phosphate crystalline phases that were identified in each of the four fractions using the computerized search-match routine. As stated above, the list is extensive and it is unlikely that all the listed phases are present. In the untreated and unleached residues, a few apatite family minerals (e.g. $Ca_5(P,Si,S)O_{12}(Cl,OH,F)$, chlorellestadite and $Ca_{10}(PO_4)_3(CO_3)_3(OH)_2$, carbonate apatite) and $CaHPO_4$ (monetite) are observed. This is likely given the presence of phosphorus in the untreated residue. These phases are generally absent after leaching. After treatment with the soluble phosphate, a large number of potential phosphate mineral phases are observed, including apatite family minerals (e.g. $Ca_5(P,Si,S)O_{12}(Cl,OH,F)$, $Ca_{10}(PO_4)_3(CO_3)_3(OH)_2$), tertiary metal phosphates (e.g. α- $CaZn_2(PO_4)_2$, $Zn_3(PO_4)_2$), and more complex phosphate minerals. Ca, Al, Zn, Fe, K, Pb, and Cd phosphate minerals are seen. Particularly noteworthy minerals for Pb are $Pb_4O(PO_4)_2$, and two apatite-family minerals: $Pb_5(PO_4)_3OH$ (lead hydroxypyromorphite), and $KPb_4(PO_4)_3$. After leaching, many of the same phosphate minerals remain; indicating their relative stability to aggressive leaching environments.

**$^{31}$P Chemical Environment Based on MAS-NMR**

The treated and unleached and treated and leached spectra are found in Figure 3a and 3b, respectively. Table 5 summarizes the data from the Herzfeld-Berger (deGroot program[43]) analysis of the spectra.

The $^{31}$P MAS NMR spectrum of the treated and unleached fraction was acquired at 2,4 and 6 kHz spin rates. The faster spin rates enable better detection of small differences in the isotropic chemical shift, while the slower spin rates yield more sidebands and should, in principal, be easier to fit. One problem that can be encountered is an isotropic chemical shift that occurs at the same frequency as the sideband from another resonance. This did not occur (see Table 5), but a fit of the 6 kHz data with a two component model showed a convergence to an isotropic chemical shift at the spinning sideband of a neighboring resonance leading us to discount the two component model for the 6 kHz data. The spectra for the 2 and 4 kHz data were both filled to two component models (see Figure 3a for the 4 kHz data); the quality of the fit was better for the 4 kHz data based on the smaller residual.

The closest match between the 4 kHz major component in the treated and unleached spectrum and likely calcium phosphate minerals[61] appears to be with a mixture of minerals with isotropic chemical shifts near 0 ppm. A mixture containing $CaHPO_4 \cdot 2H_2O$ (brushite), $CaHPO_4$ (monetite), $Ca_5(PO_4)_3OH$ (calcium hydroxyapatite), and α-$CaZn_2(PO_4)_2$ would lead to a good match with the major component with central transitions near 0 ppm and $|\Delta\delta|$ from 27 to 103 ppm. These minerals were detected by both

XRPD and XPS (see below). The three calcium phosphates also belong to the generalized Ca-phosphate precipitation reaction sequence.[28]

The closest match between the 4 kHz minor component in the treated and unleached spectra and likely calcium phosphate minerals[61] is $Ca_2P_2O_7$ or another pyrophosphate (e.g. $Na_4P_2O_7$). The minor component has a very large $|\Delta\delta|$ of 181 ppm. To our knowledge, this is one of the largest $^{31}P$ chemical shift anisotropies seen, and it indicates a distorted coordination geometry at phosphorus with non-ideal O-P-O bond angles. This conclusion is based on the correlation of $|\Delta\delta|$ with O-P-O bond angle as reported by Oldfield and coworkers.[62]

The $^{31}P$ MAS NMR spectrum of the treated and leached fraction (Figure 3b) was acquired at 6 kHz. A two component fit was used with some residuals present. Based on the intensity of the $^{31}P$ signal and the spectral side band intensity; it is obvious that the four likely major components were susceptible to aggressive leaching during the Total Availability Leaching test at pH 4.

The closest match between the 6 kHz major component in the treated and leached spectrum and likely calcium phosphate minerals[61] is $CaHPO_4 \cdot 2H_2O$ (brushite), a mineral also seen by MAS-NMR in the treated and unleached fraction (see Table 5). The closest match between the 6 kHz minor component in the treated and leached spectrum and likely calcium phosphate minerals[61] is $Ca_2P_2O_7$; a mineral also seen by XPS.

**Crystalline and Amorphous Surface Phosphate Phases Based on XPS**

As shown in Table 6, there are a number of crystalline phosphate phases found in the surface layers of the residues. In the untreated and unleached fraction, only a few phases were identified. After leaching, and with subsequent improvement in detection limit, some small quantities of apatite family (e.g. $Ca_5(PO_4)_3OH$, $Ca_5(PO_4)_3Cl$) and tertiary metal phosphate ($Ca_3(PO_4)_2$, $Pb_3(PO_4)_2$) minerals were seen. However, after treatment with the $PO_4^{3-}$, significant quantities of numerous Ca and Na phases were seen; including $Ca_5(PO_4)_3OH$, $Ca_5(PO_4)_3Cl$, $Ca_2P_2O_7$, $Ca_8H_2(PO_4)_6 \cdot 5H_2O$, $CaHPO_4$, $Na_3PO_4$, and $Na_4P_2O_7$. A number of the Ca-phosphates from the generalized Ca-phosphate precipitation reaction sequence[28] were seen (e.g. $Ca_8H_2(PO_4)_6 \cdot 5H_2O$, $CaHPO_4$, and $Ca_5(PO_4)_3OH$). After leaching of the treated residues, these same Ca-phosphate phases were still seen at high levels; suggesting resistance to solubilization at pH of 4. The principal Pb phase that was observed in the treated and leached fraction was chloropyromorphite ($Pb_5(PO_4)_3Cl$).

**Total Availability Leaching Behavior**

The total availability leaching data for the untreated and treated residues are shown in Table 7. The table contains data on the concentration of the analytes in the leachate (not corrected for added weight of treatment additives) and a calculated stabilization fraction (corrected for added weight of treatment additives). The calculated stabilization fraction examines the percentage of the total available fraction in the untreated residue that was immobilized by the treatment process.

The dose of 1.2 moles of $H_3PO_4$ per kg of residue reduced the leachability of Al (75.5%), Ba (27.7%), Ca (6.8%), Cd (37.5%), Cl (7.7%), Cu (57.9%), Pb (99.5%) and Zn (28.2%). The larger reduction in Pb leaching agrees with the insoluble phases seen with XRPD and XPS.

The treatment increased the leachability of As (-3.8%), Hg (-3,979%), Mg (-19.9%), Si (-97.5%), and $PO_4^{3-}$ (-2,385%). The Hg data reflect large changes in a very small leachate concentration number. The Mg and As data reflect likely substitution reactions (Ca for Mg, $PO_4^{3-}$ for $AsO_4^{3-}$). The increased Si

concentrations reflect the dissolution of aluminosilicates by acid attack ($H_3PO_4$ addition). It is also clear that either not all of the $PO_4^{3-}$ was reacted or that some of the phases that formed were not the most thermodynamically stable ones at the pH of the Total Availability Leaching Test.

The stabilization agent has a clear positive impact on the reduction of leaching of many divalent cations ($Pb^{2+}$, $Cd^{2+}$, $Cu^{2+}$, $Zn^{2+}$) in general agreement with the formation of insoluble phases which were seen with the various spectroscopic methods. These phases are insoluble and geochemically stable even under aggressive leaching conditions.

**pH Dependent Leaching and Geochemical Modeling**

Particular attention is given here to the components $Ca^{2+}$ and $Pb^{2+}$, although similar behaviors were seen for $Cd^{2+}$, $Cu^{2+}$ and $Zn^{2+}$. The leaching of $Ca^{2+}$and $Pb^{2+}$ is shown in Figures 4 and 5, respectively. Each of the figures depicts pH-dependent leaching of the untreated and treated residues as well as the leachate concentrations in the modeled leachates when potential controlling solids were individually introduced as infinite solids in the model at each pH. As infinite solids, the candidate mineral dictates the activity of its components in the leachate in response to system pH and to all attendant aqueous phase complexation reactions. Table 8 identifies the top few controlling solids (based on their saturation indices) that were initially identified as well as other solids of interest; some of which were used as candidate infinite solids.

$Ca^{2+}$ shows a clear reduction in leaching over the entire pH range after treatment (Figure 4a). As shown in Table 8, there are a number of phases that were excellent candidates as controlling solids; particularly $CaHPO_4$ (monetite) and $CaHPO_4 \cdot 2H_2O$ (brushite). These were seen with XRPD, MAS-NMR and XPS in the treated residues whereas anhydrite and gypsum were less prevalent. As infinite solids, monetite and brushite each are able to depict $Ca^{2+}$ leaching in the treated residues (Figure 4b). Despite their high saturation indices, $Ca_5(PO_4)_3Cl$ (calcium chloroapatite) and $Ca_5(PO_4)_3OH$ (calcium hydroxyapatite) (Figure 4c) both describe the general shape and pH-trend for $Ca^{2+}$ leaching from the treated residues. While these phases were seen with XRPD, XPS, and MAS-NMR in the treated residues; they may be less suitable, but still plausible candidates for controlling solids.

The pH-dependent leaching of $Pb^{2+}$ shows 1 to 2 log reduction in leaching after treatment (Figure 5a). As with $Cu^{2+}$ and $Cd^{2+}$, a few candidate phases may control at each of the pH values (Figure 5b). These phases include apatite and tertiary metal phosphates ideal solid solutions (e.g. $(Pb_2,Ca)(PO_4)_2$, $(Pb,Ca_4)(PO_4)_3Cl$). The end member $Pb_5(PO_4)_3Cl$ (chloropyromorphite) is a controlling solid (Figure 5c) and is present in the treated and leached fraction. $PbHPO_4$ is also not a likely candidate.

**Stabilization Reaction Pathway Kinetics and Products**

The typical "ideal" solution phase reaction sequence when $PO_4^{3-}$ is titrated into a Ca-salt solution involves the sequential formation of $Ca_9(PO_4)_6$ (non-stoichiometric amorphous calcium phosphate), $CaHPO_4 \cdot 2H_2O$ (brushite), $CaHPO_4$ (monetite), $Ca_8H_2(PO_4)_6 \cdot 5H_2O$ (octacalcium phosphate), and then $Ca_5(PO_4)_3OH$ (hydroxyapatite); the thermodynamically most stable reaction product.[28] This sequence of nucleation and crystallite growth from supersaturated solutions is dependent upon system pH, temperature, the presence of "seed" crystals or catalytic surfaces, and reaction kinetics.[26] Intermediates are typically "active", geochemically labile, and dependent upon reaction kinetics. Under ideal conditions, hydroxyapatite is the most thermodynamically stable end product over a fairly wide pH range (e.g. 4 to above 8).[26]

The more complex stabilization system studied here is similar in principal to the one just described. $PO_4^{3-}$ is titrated into a Ca-salt dominated waste. While the L/S ratio is much less than the "ideal" system, there is evidence that the same reaction sequence is observed here. The minerals brushite, monetite and calcium hydroxyapatite were seen in the treated residues with XRPD, MAS-NMR or XPS. Data also suggest that the initial 10 minute mixing scenario at pH values above 12 was not sufficient time to allow for complete conversion of all Ca-phosphates to apatites. Not only were intermediaries seen, but subsequent paragenic transformations occurred during the seven hours of the Total Availability Leaching test at pH 7 and then 4. To optimize the stabilization process, more process water and longer reaction times might be preferred. Nevertheless, despite the short reaction times, significant reductions in metals leachability and formations of more stable reaction products were seen. For instance, the dissolution of calcium hydroxyapatite in the presence of $Pb^{2+}$ and the subsequent formation of "mature" lead chloropyromorphite can take place on the order of minutes to hours provided liquid-to-solid ratios are high and pH is in the neutral region.[17,18,19,20]

The pH-dependent leaching modeling shows that for $Cd^{2+}$, $Cu^{2+}$,$Pb^{2+}$ and $Zn^{2+}$; ideal solid solutions of Ca-apatites (both hydroxyapatite and chloroapatite) and whitlockite were found to adequately describe pH-dependent leaching. Neither Ca-apatites nor whitlockite controlled $Ca^{2+}$ leaching; yet these phases were detected with XRPD, XPS, and MAS-NMR; particularly the highly substituted apatite mineral chlorellestadite. It may be reasonable to assume that the solid solutions that were found to control leaching (e.g. $(Cd, Ca_4)(PO_4)_3OH$; $(Cu, Ca_4)(PO_4)_3OH$, $(Pb, Ca_4)(PO_4)_3OH$) were in fact present and controlling leaching but that the degree of isostructural substitution was small enough as to not interfere with their detection using crystallographic or nearest-neighbor spectroscopic signatures.

This is consistent with the premise that major-minor cation solid solutions limit the concentration of the minor component to levels below saturation of the minor cation end member.[63] Formation of these types of solid solutions allows for the "burial" of the minor cation in the Ca-apatites or whitlockite. These solid solutions can be easily formed from saturated solutions[34,35] and it is reasonable to infer that this process occurred here.

The very small particle sizes of the reaction products as seen with STEM (100-5,000 nm) suggests that Ostwald ripening processes must also be considered. Nanometer-sized crystallites are many orders of magnitude more soluble than larger, ripened crystals.[28] Such phenomenon have been theorized[64] and modelled[65,66] for Ca-phosphates. At crystallite sizes less than 500 nm, particle interfacial tensions increase solubilities exponentially.[28,68] It is therefore also possible that some of the positive saturation indices seen for some of the major cation end members could be explained by incomplete ripening and overly "active" small crystal solubilities. If this is the case, then, the allowance for longer reaction times and more process water would ensure crystallite growth, aggregation, and maturation. This would help further decrease equilibrium leachate concentrations of $Cd^{2+}$, $Cu^{2+}$, $Pb^{2+}$, and $Zn^{2+}$ and further increase the fraction stabilized during treatment.

**Implications for the Waste-to-Energy Industry**

Chemical stabilization of dry scrubber residue using soluble phosphate is an effective means of immobilizing divalent metals in the waste. The treatment process holds promise for the industry. Knowledge about the fundamental immobilization mechanism allows for further optimization of the process. Successful identification of geochemically stable and insoluble reaction products using numerous spectroscopic methods confirms the role of the apatite mineral family as the dominant reaction product. Geochemical modeling also showed the importance of these minerals in controlling leaching of divalent metals. Such modeling techniques can be used as predictive tools for refining treatment

formulations, examining long term disposal behavior of treated residues, and developing management strategies for the treated residues.

## CONCLUSIONS

The use of soluble orthophosphate as a heavy metal chemical stabilization agent was evaluated for a calcium-based scrubber residue from the combustion of municipal solid waste. At an experimental dose of 1.2 moles of $H_3PO_4$ per kg of residue, the reduction in the fraction available for leaching (using the Total Availability Leaching test) is 38% for Cd, 58% for Cu, 99% for Pb and 28% for Zn. pH-dependent leaching (pH 4,6,8) showed that the treatment was able to reduce equilibrium concentrations by 0.5 to 3 log units for many of these metals; particularly Pb. Numerous spectroscopic techniques were used to identify stabilization reaction mechanisms and reaction products both prior to and after Total Availability Leaching. Depth profiling of particles with secondary ion mass spectroscopy (SIMS) suggests that stabilization is by discrete heterogeneous phases precipitation rather than by adsorption. Scanning transmission electron microscopy/x-ray microanalysis (STEM/XRM), x-ray powder diffraction (XRPD), magic angle spinning-nuclear magnetic resonance (MAS-NMR), and x-ray photoelectron spectroscopy (XPS) suggest that the insoluble metal phosphate reaction products are small (nm-sized) crystalline and amorphous precipitates and that calcium phosphates, tertiary metal phosphates, and apatite family minerals are dominant reaction products. Observed phases include $CaHPO_4 \cdot 2H_2O$ (brushite), $CaHPO_4$ (monetite), $\beta$-$Ca_3(PO_4)_2$ (whitlockite), $Ca_5(PO_4)_3OH$ (hydroxyapatite); $CaZn_2(PO_4)_2$; and $Pb_5(PO_4)_3Cl$ (lead chloropyromorphite); many of which are geochemically stable. The geochemical thermodynamic equilibrium model MINTEQA2 was modified to include both extensive phosphate minerals and ideal divalent cation binary solid solutions for modeling solid phase control of leaching. Both end members (e.g. $CaHPO_4$, $CaHPO_4 \cdot 2H_2O$) and ideal solid solutions (e.g. $(Pb,Ca_4)(PO_4)_3Cl$, $CaZn_2(PO_4)_2 \cdot 2H_2O$) were seen to act as controlling solids for $Ca^{2+}$, $Zn^{2+}$, $Pb^{2+}$, $Cu^{2+}$, and $Cd^{2+}$. The formation of solid solutions is both plausible and highly likely in this system and describes a mechanism whereby minor cation components (e.g. $Cd^{2+}$, $Cu^{2+}$, $Pb^{2+}$, $Zn^{2+}$) are "buried" in the precipitating calcium phosphate reaction product. However, issues related to Ostwald ripening and small reaction product particle size may also explain some of the observed leaching behavior. Soluble phosphate is an effective stabilization agent for divalent metal cations in waste materials such as scrubber residues.

## ACKNOWLEDGEMENTS

This work was supported by a research contract from Wheelabrator Environmental Systems Inc. and Kurita Water Industries Ltd. We thank Nan Collins, Dr. Henri Gaudette and Dr. Ted Loder of UNH; Dr. Milenko Markovic of NIST; George Bruno of AMRAY Inc.; Dr. Sheldon Landsberger and Dr. Wesley Wu of the University of Illinois at Champaign-Urbana; Brian Hart of the University of Western Ontario; Rusty Foster and Bud Berry of Resource Laboratories Inc.; and Tim Wilson of Eastern Analytical Inc. for their assistance in this effort. The financial support for the Analytical Shared Experimental Facility at the Center for Materials Science and Engineering at MIT comes from NSF grant DMR90-22933.

## LITERATURE CITED

1. T.T. Eighmy, S.F. Bobowski, T.P. Ballestero, M.R. Collins, in "Theoretical and applied methods of lead and cadmium stabilization in combined ash and scrubber residues," Proceedings of the Second International Conference on Municipal Solid Waste Combustor Ash Utilization, W.H. Chesner, T.T. Eighmy, Eds., UNH Press, Durham, N.H., 1990, pp 275-314.

2. T.T. Eighmy, B.S. Crannell, J.R. Krzanowski, J.D. Eusden, L.G. Butler, F.K. Cartledge, E. Emery, E.L. Shaw, C.A. Francis, "Fundamental mechanisms of phosphate stabilization in granular waste materials," Abstract ANYL 186, 211th ACS National Meeting, New Orleans, Louis., March 24-28, 1996.

3. T.T. Eighmy, B.S. Crannell, J.R. Krzanowski, J.D. Eusden, L.G. Butler, F.K. Cartledge, E. Emery, E.L. Shaw, C.A. Francis, "The use of surface analysis and geochemical modeling to describe leaching behavior in chemically-stabilized particulate waste residues," Abstract 169, 70th Colloid and Surface Science Symposium, Clarkson University, Postdam, N.Y., June 16-19, 1996.

4. V. Laperche, P. Gaddam, S.J. Traina, "Immobilization of lead by apatite," Abstract GEOC 087, 211th ACS National Meeting, New Orleans, Louis., March 24-28, 1996.

5. J. Wright, J. Conca, T. Moody, X. Chen, "Immobilization of metals using apatite minerals: precipitation or sorption?," Abstract GEOC 088, 211th ACS National Meeting, New Orleans, Louis., March 24-28, 1996.

6. W.L. Lindsay, and P.L. Vlek, Minerals in Soil Environments; J.B. Dixon, Ed. Soil Science Society of America, Madison, Wisconsin, 1977. pp 639-672.

7. J.O. Nriagu, Phosphate Minerals; J.O. Nriagu, P.B. Moore, Eds. Springer-Verlag: Berlin, 1984, pp 318-329.

8. W.L. Lindsay and E.C. Moreno, "Phosphate phase equilibria in soils," Soil Sci. Soc. Amer. Proc., 24: 177-182 (1960).

9. J.J. Jurniak and T.S. Inouye, "Some aspects of zinc and copper phosphate formation in aqueous systems," Soil Sci. Soc. Amer. Proc., 26: 144-147 (1962).

10. J.O. Nriagu, "Lead orthophosphates. IV: formation and stability in the environment," Geochim. Cosmochim. Acta., 38: 887-898 (1974).

11. J. Santillan-Medrano and J.J. Jurinak, "The chemistry of lead and cadmium in soil: solid phase formation," Soil Sci. Soc. Amer. Proc., 39: 851-856 (1975).

12. J.J. Street, W.L. Lindsay and B.R. Sabey, "Solubility and plant uptake of cadmium is soils amended with cadmium and sewage sludge," J. Environ. Qual., 6: 72-77 (1977).

13. M.V. Ruby, A. Davis and A. Nicholson, "In situ formation of lead phosphates in soils as a method to immobilize lead," Environ. Sci. Technol., 28: 646-654 (1994).

14. J.O. Nriagu, "Lead orthophosphates.II: stability of chloropyromorphite at 25°C," Geochim. Cosmochim. Acta., 37: 367-377 (1973).

15. Y. Takeuchi and H. Arai, "Removal of coexisting $Pb^{2+}$, $Cu^{2+}$ and $Cd^{2+}$ ions from water by addition of hydroxyapatite powder," J. Chem. Eng. Japan, 23: 75-80 (1990).

16. V. Laperche, S.J. Traina, P. Gaddam and T.J. Logan, "Chemical and mineralogical characterizations of Pb in a contaminated soil: reactions with synthetic apatite," Environ. Sci. Technol., 30: 3321-3326 (1996).

17. Q.Y. Ma, S.J. Traina, T.J. Logan and J.A. Ryan, "In situ lead immobilization by apatite," Environ. Sci. Technol., 27: 1803-1810 (1993).

18. Q.Y. Ma, T.J. Logan, S.J. Traina and J.A. Ryan, "Effects of $NO_3^-$, $Cl^-$, $F^-$, $SO_4^{2-}$, and $CO_3^{2-}$ on $Pb^{2+}$ immobilization by hydroxyapatite," Environ. Sci. Technol., 28: 408-418 (1994).

19. Q.Y. Ma, S.J. Traina, T.J. Logan and J.A. Ryan, "Effects of aqueous Al, Cd, Cu, Fe(II), Ni and Zn on Pb immobilization by hydroxyapatite," Environ. Sci. Technol., 28: 1219-1228 (1994).

20. Q.Y. Ma, T.J. Logan and S.J. Traina, "Lead immobilization from aqueous solutions and contaminated soils using phosphate rocks," Environ. Sci. Technol., 29: 1118-1126 (1995).

21. M.B. McBride, Environmental Chemistry of Soils, Oxford University Press, New York, 1990.

22. R.B. Corey, Adsorption of Inorganics at Solid-Liquid Interfaces, M.A. Anderson, A.J. Rubin, Eds. Ann Arbor Science, Ann Arbor, Michigan, 1981, pp 161-182.

23. K.J Farley, D.A. Dzombak and F.M.M. Morel, "A surface precipitation model for the sorption of cations on metal oxides," J. Colloid Interface Sci., 106: 226-242 (1985).

24. J.E. Fulghum, S.R. Bryan, R.W. Linton, C.F. Bauer and D.P. Griffis, "Discrimination between adsorption and coprecipitation in aquatic particle standards by surface analysis techniques: lead distributions in calcium carbonates," Environ. Sci. Tech., 22: 463-467 (1988).

25. G. Sposito, Geochemical Processes at Mineral Surfaces; J.A. Davis, K.F. Hayes, Eds. ACS, Washington, D.C., 1986, pp 217-228.

26. G.H. Nancollas, Phosphate Minerals; J.O. Nriagu, P.B. Moore, Eds. Springer-Verlag, Berlin, 1984, pp 137-154.

27. P. van Cappellen, and R.A. Bernier, Water-Rock Interaction; D. Miles Ed. Rotterdam, the Netherlands, 1989, pp 707-710.

28. J.W. Morse and W.N. Casey, "Ostwald processes and mineral paragenesis in sediments," Am. J. Sci., 288: 537-560 (1988).

29. J. Cristofferson, M.R. Christoffersen, W. Kibalczyc and F.A. Andersen, "A contribution to the understanding of the formation of calcium phosphates," Crys. Growth, 94: 767-777 (1989).

30. J.J. Middleburg and R.N.J. Comans, "Sorption of cadmium on hydroxyapatite," Chem. Geol., 90: 45-53 (1991).

31. D.N. Misra, R.L. Bowen and B.M. Wallace, "Adhesive bonding of various materials to hard tooth tissues. VII Nickel and copper ions on hydroxyapatite; role of ion exchange and surface nucleation," J. Colloid Interface Sci., 51: 36-43 (1975).

32. D.N. Misra and R.L. Bowen, Adsorption and Surface Chemistry of Hydroxyapatite; D.N. Misra, Ed. Plenum Press, New York, N.Y, 1984, pp 169-175.

33. Y. Xu, F.W. Schwartz and S.J. Traina, "Sorption of $Zn^{2+}$ and $Cd^{2+}$ on hydroxyapatite surfaces," Environ. Sci. Technol., 28: 1472-1480 (1994).

34. A. Panda, B. Sahu, P.N. Patel and B. Mishra, "Hydroxylapatite solid solutions: preparation, infrared and lattice constant measurements," Transition Met. Chem., 16: 476-477 (1991).

35. M. Pujari and P.N. Patel, "Strontium-copper-Calcium hydroxyapatite solid solutions: preparation, infrared, and lattice constant measurements," Solid State Chem., 83: 100-104 (1989).

36. International Ash Working Group (IAWG), Municipal Solid Waste Incinerator Residues. An International Perspective on Their Characteristics, Disposal, Treatment and Utilization, Summary Report, Netherlands Energy Research Foundation: Petten, the Netherlands, 1994.

37. T.T. Eighmy, J. Krzanowski, D. Domingo, D. Stämpfli, J.D. Eusden, Jr., K. Marsella, K. Killeen, H. Gardenier and J. Hogan, The Nature of Lead, Cadmium and Other Elements in Incineration Residues and Their Stabilized Products, U.S. EPA Final Report, U.S. Environmental Protection Agency, Washington, D.C. (in press).

38. T.T. Eighmy, J.D. Eusden, Jr., J.E. Krzanowski, D.S. Domingo, D. Stämpfli, J.R. Martin and P.M. Erickson, "A comprehensive approach towards understanding element speciation and leaching behavior in municipal solid waste incineration electrostatic precipitator ash," Environ. Sci. Technol., 29: 629- 646 (1995).

39. B.A. Buchholz and S. Landsberger, "Trace metal analysis of size-fractionated municipal solid waste incineration fly ash and its leachates," J. Environ. Sci. Health, A28: 423-441 (1993).

40. S. Landsberger, B.A. Buchholz, M. Kaminski and M. Plewa, "Trace Elements in Municipal Solid Waste Incineration Fly Ash," J. Radioanal. Nucl. Chem., 167: 331-340 (1993).

41. I.L. Mudrakovskii, V.P. Shmachkova, N.S. Kotsarenko and V.M. Mastikhin, "Phosphorus-31 NMR study of polycrystalline phosphates of group I-IV elements," J. Phys. Chem. Solids, 47: 335-339 (1986).

42. J. Herzfeld and A.E. Berger, "Sideband intensities in NMR spectra of samples spinning at the magic angle," J. Chem. Phys., 73: 6021-6030 (1980).

43. H.J.M. de Groot, S.O. Smith, A.C. Kolbert, M.M.L. Courtin, C. Winkel, J. Lugtenberg, J. Herzfeld and P.G. Griffin, "Iterative fitting of magic angle spinning NMR spectra," J. Magn. Reson., 91: 30-38 (1991).

44. T.L. Barr and S. Seal, "Nature of the use of adventitious carbon as a binding energy standard," J. Vac. Sci. Tech., A13: 1239-1246 (1995).

45. D. Briggs and M.P. Seah, Practical Surface Analysis, J. Wiley & Sons, Chichester, U.K., 1990.

46. J.F. Moulder, W.F. Stickle, P.E. Sobol, et al., Handbook of X-ray Photoelectron Spectroscopy, Perkin Elmer Corp., Eden Prairie, Minn, 1992.

47. C.J. Powell and M.P. Seah, "Precision, accuracy, and uncertainty in quantitative surface analyses by Auger-electron spectroscopy and x-ray photoelectron spectroscopy," J. Vac. Sci. Tech., A8: 735-763 (1990).

48. H.A. van der Sloot, D. Hoede and P. Bonouvrie, Comparison of Different Regulatory Leaching Test Procedures for Waste Materials and Constuction Materials, ECN-C-91-082, Netherlands Energy Research Foundation: Petten, the Netherlands, 1991.

49. U.S. EPA, Methods for Chemical Analysis of Water and Wastes, EPA-600/4-79-020, U.S. Environmental Protection Agency, Washington, D.C., 1979.

50. U.S. EPA, Test Methods for Evaluating Solid Waste-Physical/Chemical Methods, U.S. EPA SW846; U.S. Environmental Protection Agency, Washington, D.C., 1984.

51. American Public Health Association, Standard Methods for the Examination of Waters and Wastewaters, 16th ed., APHA, Washington, D.C., 1989.

52. G. Faure, Principles of Isotope Geology, John Wiley & Sons, New York, N.Y., 1986.

53. Lachat Instruments, Phosphate in Brackish Seawater, QuikChem Method 31-115-01-3-a, Lachat Instruments, Milwaukee, Wisconsin, 1994.

54. J.D. Allison, D.S. Brown and K.K. Novo-Gradac, MINTEQA2/PRODEFA2, A Geochemical Assessment Model for Environmental Systems: Version 3.0 User's Manual, Environmental Research Laboratory, U.S. Environmental Protection Agency, Athens, Georgia, 1990.

55. J.O. Nriagu, "Phosphate-clay mineral relations in soils and sediments," Can. J. Earth Sci., 13: 717-736 (1976).

56. P. Viellard and Y. Tardy, Phosphate Minerals; J.O. Nriagu and P.B. Moore, Eds. Springer-Verlag, Berlin, 1984, pp 171-198.

57. D.T. Rickard and J.O. Nriagu, The Biochemistry of Lead in the Environment; J.O. Nriagu, Ed. Elsevier/North-Holland Biomedical Press, Amsterdam, 1978, pp 219-284.

58. D.D. Wagman, W.H. Evans, V.P. Parker, R.H. Schumm, I. Halow, S.M. Bailey, K.L. Churney and R.L. Nuttall, "The NBS tables of chemical thermodynamic properties: selected values for inorganic and $C_1$ and $C_2$ organic substances in SI units," J. Phys. Chem. Ref. Data, 11(2): 2-1 - 2-392 (1982).

59. A. Davis, M.V. Ruby, M. Bloom, R. Schoof, G. Freeman and P.D. Bergstrom, "Mineralogical constraints on the bioavailability of arsenic in smelter-impacted soils," Environ. Sci. Technol., 30: 392-399 (1996).

60. H.J. Greenwood, Short Course in Application of Thermodynamics to Petrology and Ore Deposits; H.J. Greenwood, Ed. Mineralogical Association of Canada, Toronto, 1977, pp 38-46.

61. T.M. Duncan, A Compilation of Chemical Shift Anisotropies, Farragut Press, Madison, Wisconsin, 1990.

62. G.L. Turner, K.A. Smith, R.J. Kirkpatrick and E. Oldfield, "Structure and cation effects on phosphorus-31 NMR chemical shifts and chemical shift anisotropies of orthophosphates," J. Magn. Reson., 70: 408-415 (1986).

63. D. Langmuir, Aqueous Environmental Geochemistry, Prentice Hall, Upper Saddle River, New Jersey, 1997.

64. F.C. Smales, Tooth Enamel II, its composition, properties and fundamental structure; R.W. Fernhead and M.V. Stack, Eds. John Wright & Sons, Bristol, England, 1971, pp 187-191.

65. T.P. Feenstra and P.L. De Bruyn, "The Ostwald rules of stages in precipitation from highly supersaturated solutions: a model and its application to the formation of nonstoichiometric amorphous calcium phosphate precursor phase," J. Colloid Inter. Sci., 84: 66-72 (1981).

66. C.I. Steefel and P. van Cappellen, "A new kinetic approach to modeling water-rock interaction: the role of nucleation, precursors, and Ostwald ripening," Geochim. Cosmochim. Acta, 54: 2657-2677 (1990).

Table 1. Some Divalent Metal Phosphate Minerals and Their Solubility Products

| Mineral Name | Dissolution Reaction | | | -Log $K_{sp}$ | $\Delta G_f^o$ | Reference |
|---|---|---|---|---|---|---|
| Apatites | | | | | | |
| Hydroxyapatite | $Ca_5(PO_4)_3OH + H^+$ | <=> | $5Ca^{2+} + 3PO_4^{3-} + H_2O$ | 38.15 | -6,279.0 | (a) |
| Chloroapatite | $Ca_5(PO_4)_3Cl$ | <=> | $5Ca^{2+} + 3PO_4^{3-} + Cl^-$ | 46.89 | -6,223.0 | (b) |
| Hydroxypyromorphite | $Pb_5(PO_4)_3OH + H^+$ | <=> | $5Pb^{2+} + 3PO_4^{3-} + H_2O$ | 62.80 | -3,774.0 | (b) |
| Chloropyromorphite | $Pb_5(PO_4)_3Cl$ | <=> | $5Pb^{2+} + 3PO_4^{3-} + Cl^-$ | 84.43 | -3,791.5 | (b) |
| $Cd_5(PO_4)_3OH$ | $Cd_5(PO_4)_3OH + H^+$ | <=> | $5Cd^{2+} + 3PO_4^{3-} + H_2O$ | 42.49 | -3,924.0 | (a) |
| $Cd_5(PO_4)3Cl$ | $Cd_5(PO_4)_3Cl$ | <=> | $5Cd^{2+} + 3PO_4^{3-} + Cl^-$ | 49.66 | -3,859.0 | (b) |
| $Zn_5(PO_4)3$ OH | $Zn_5(PO_4)_3OH + H^+$ | <=> | $5Zn^{2+} + 3PO_4^{3-} + H_2O$ | 49.10 | -4,309.0 | (c) |
| $Zn_5(PO_4)_3Cl$ | $Zn_5(PO_4)_3Cl$ | <=> | $5Zn^{2+} + 3PO_4^{3-} + Cl^-$ | 37.53 | -4,137.0 | (a) |
| $Cu_5(PO_4)_3OH$ | $Cu_5(PO_4)_3OH + H^+$ | <=> | $5Cu^{2+} + 3PO_4^{3-} + H_2O$ | 51.62 | -6,279.0 | (c) |
| $Cu_5(PO_4)_3Cl$ | $Cu_5(PO_4)_3Cl$ | <=> | $5Cu^{2+} + 3PO_4^{3-} + Cl^-$ | 53.96 | -3,168.0 | (a) |
| Tertiary Metal Phosphates | | | | | | |
| Low Whitlockite | $\beta$-$Ca_3(PO4)_2$ | <=> | $3Ca^{2+} + 2PO_4^{3-}$ | 32.69 | -3,884.8 | (b) |
| $Pb_3(PO_4)_2$ | $Pb_3(PO4)_2$ | <=> | $3Pb^{2+} + 2PO_4^{3-}$ | 44.36 | -2,364.0 | (d) |
| $Zn_3(PO_4)_2$ | $Zn_3(PO4)_2$ | <=> | $3Zn^{2+} + 2PO_4^{3-}$ | 27.11 | -2,633.4 | (b) |
| $Cu_3(PO4)_2$ | $Cu_3(PO4)_2$ | <=> | $3Cu^{2+} + 2PO_4^{3-}$ | 36.85 | -2,051.6 | (b) |
| $Cd_3(PO4)_2$ | $Cd_3(PO4)_2$ | <=> | $3Cd^{2+} + 2PO_4^{3-}$ | 32.60 | -2,456.3 | (b) |
| $Mg_3(PO4)_2$ | $Mg_3(PO4)_2$ | <=> | $3Mg^{2+} + 2PO_4^{3-}$ | 24.38 | -3,538.8 | (b) |
| Tetra Metal Phosphates | | | | | | |
| Hilgenstockite | $Ca_4O(PO_4)_2 + 2H^+$ | <=> | $4Ca^{2+} + 2PO_4^{3-} + H_2O$ | 17.36 | -4,588.0 | (b) |
| $Pb_4O(PO_4)_2$ | $Pb_4O(PO_4)_2 + 2H^+$ | <=> | $4Pb^{2+} + 2PO_4^{3-} + H_2O$ | 36.86 | -2,582.8 | (b) |
| Other Phosphate Minerals | | | | | | |
| $AlPO_4$ | $AlPO_4$ | <=> | $Al^{3+} + PO_4^{3-}$ | 17.00 | -1,601.2 | (b) |
| Monetite | $CaHPO_4$ | <=> | $Ca^{2+} + PO_4^{3-} + H^+$ | 19.09 | -1,681.2 | (e) |
| Brushite | $CaHPO_4 \cdot 2H_2O$ | <=> | $Ca^{2+} + PO_4^{3-} + 2H_2O + H^+$ | 18.93 | -2,154.8 | (b) |
| Cornetite | $Cu_3PO_4(OH)_3 + 3H^+$ | <=> | $3Cu^{2+} + PO_4^{3-} + 3H_2O$ | 5.94 | -1,567.7 | (c) |
| Libethenite | $Cu_2PO_4OH + H^+$ | <=> | $2Cu^{2+} + PO_4^{3-} + H_2O$ | 14.00 | -1,204.9 | (c) |
| Pseudomalachite | $Cu_5(PO_4)_2(OH)_4 + 4H^+$ | <=> | $5Cu^{2+} + 2PO_4^{3-} + 4H_2O$ | 19.83 | -2,771.9 | (c) |
| Corkite | $PbFe_3(PO_4)(OH)_6SO_4 + 6H^+$ | <=> | $Pb^{2+} + 3Fe^{3+} + PO_4^{3-} + SO_4^{2-} + 6H_2O$ | 28.66 | -3,388.2 | (c) |
| Spencerite | $Zn_4(PO_4)_2(OH)_2AlPO_4 \cdot 3H_2O + 2H^+$ | <=> | $4Zn^{2+} + 2PO_4^{3-} + 5H_2O$ | 24.77 | -3,953.0 | (c) |
| Zn Rockbridgite | $ZnFe_4(PO_4)_3(OH)_5 + 5H^+$ | <=> | $Zn^{2+} + 4Fe^{3+} + 3PO_4^{3-} + 5H_2O$ | 68.55 | -4,799.0 | (c) |
| Scholzite | $CaZn_2(PO_4)_2 \cdot 2H_2O$ | <=> | $Ca^{2+} + 2Zn^{2+} + 2PO_4^{3-} + 2H_2O$ | 34.10 | -3,553.5 | (c) |
| Tarbuttite | $Zn_2(PO_4)OH + H^+$ | <=> | $2Zn^{2+} + PO_4^{3-} + H_2O$ | 12.55 | -1,621.7 | (c) |
| Faustite | $ZnAl_6(PO_4)_4(OH)_8 \cdot 4H_2O + 8H^+$ | <=> | $Zn^{2+} + 6Al^{3+} + 4PO_4^{3-} + 12H_2O$ | 65.70 | 10,355.4 | (c) |
| Plumbogummite | $PbAl_3(PO_4)_2(OH)_5 \cdot H2O + 5H^+$ | <=> | $Pb^{2+} + 3Al^{3+} + 2PO_4^{3-} + 6H_2O$ | 29.36 | -5,108.7 | (c) |
| Hinsdalite | $PbAl_3(PO_4)(SO_4)(OH)_6 + 6H^+$ | <=> | $Pb^{2+} + 3Al^{3+} + PO_4^{3-} + SO_4^{2-} + 6H_2O$ | 15.10 | -4,753.0 | (d) |
| Tsumebite | $CuPb_2(PO_4)(OH)_3 \cdot 3H_2O + 3H^+$ | <=> | $Cu^{2+} + 3Pb^{2+} + PO_4^{3-} + 6H_2O$ | 9.36 | -2,478.6 | (d) |

[a] Estimated by method of Nriagu[55]

[b] Veillard and Tardy[56]

[c] Nriagu[7]

[d] Rickard and Nriagu[57]

[e] Wagman et al.[58]

Table 2. Total Elemental Composition for Dry Scrubber Residue

| Element | Concentration mg/kg error | Element | Concentration mg/kg error |
|---|---|---|---|
| Ag | 19.6 ± 0.3 | Mn | 385.9 ± 19.0 |
| Al | 29,600 ± 2,100 | Mo | 29.2 ± 3.5 |
| As | 46.0 ± 4.8 | Na | 14,500 ± 900 |
| Au | 0.25 ± 0.01 | Nd | 5.55 ± 0.79 |
| Ba | 449.3 ± 95 | Ni | 49.5 ± 8.4 |
| Br | 1,550 ± 130 | O | ~300,000 |
| C | ~70,000 | P | 2,100 ± 200 |
| Ca | 354,400 ± 11,400 | Pb | 1,990 ± 6 |
| Cd | 99.3 ± 6.8 | Rb | 26.9 ± 1.8 |
| Ce | 12.8 ± 0.4 | S | 19,800 ± 1,000 |
| Cl | 118,400 ± 6,000 | Sb | 473.5 ± 28.1 |
| Co | 9.43 ± 0.13 | Sc | 1.88 ± 0.02 |
| Cr | 131.8 ± 1.3 | Se | 3.07 ± 0.52 |
| Cs | 1.42 ± 0.08 | Si | 42,100 ± 4,900 |
| Cu | 362.1 ± 2.5 | Sm | 0.91 ± 0.09 |
| Dy | 1.53 ± 0.52 | Sr | < 538 |
| Eu | 0.25 ± 0.04 | Ta | 0.36 ± 0.05 |
| Fe | 6,570 ± 107 | Tb | < 0.13 |
| Hf | 2.26 ± 0.07 | Th | 1.93 ± 0.06 |
| Hg | 31.4 ± 0.3 | Ti | 6,090 ± 400 |
| In | 0.79 ± 0.07 | U | < 1.80 |
| I | 25.6 ± 13.1 | V | < 12.3 |
| K | < 7,500 | W | 5.78 ± 0.72 |
| La | 6.83 ± 0.77 | Yb | < 0.41 |
| Mg | 5,200 ± 1,700 | Zn | 11,770 ± 70 |
| | | Zr | 125.5 ± 28.1 |

Table 3. Particle Atomic Concentrations (%) Based on STEM-XRM Analyses

| Fraction | Particle Number | O | Mg | Al | Si | P | S | Cl | K | Ca | Fe | Zn | Pb |
|---|---|---|---|---|---|---|---|---|---|---|---|---|---|
| **Treated and Unleached** | 1 | 39.1 | - | 13.1 | - | - | - | 30.2 | - | 17.6 | - | - | - |
| | 2 | 59.7 | - | 5.1 | - | - | - | 10.8 | - | 24.0 | - | - | - |
| | 3 | 78.3 | - | - | - | - | 9.9 | 0.3 | - | 11.5 | - | - | - |
| | 4 | 31.9 | - | - | 0.8 | 7.2 | 5.8 | 12.2 | - | 42.8 | - | - | - |
| | 5 | 42.0 | 2.4 | 3.3 | 6.3 | 4.2 | 2.3 | 13.5 | 1.1 | 19.2 | - | - | - |
| | 6 | 45.7 | 0.8 | 0.9 | 1.3 | 2.1 | 15.5 | 4.8 | 0.8 | 27 3 | - | - | - |
| | 7 | 32.0 | 0.6 | 5.6 | 0.5 | 0.8 | 1.9 | - | - | 58.0 | - | - | - |
| | 8 | 54.6 | - | - | - | - | - | 22.6 | 0.6 | 22.0 | - | - | - |
| | 9 | 55.9 | - | - | - | - | - | 21.6 | - | 22.6 | - | - | - |
| | 10 | 14.6 | 5.3 | 2.9 | 4.4 | 7.0 | 6.1 | 16.5 | 0.8 | 42.4 | - | - | - |
| **Treated and Leached** | 1 | 71.2 | 0.9 | 9.8 | 1.9 | 4.9 | 2.8 | - | - | 6.1 | 0.7 | 0.7 | - |
| | 2 | 40.1 | 0.8 | - | - | 19.9 | 3.6 | - | - | 31.3 | 1.5 | 2.2 | - |
| | 3 | 17.7 | - | 5.2 | - | 28.1 | 1.8 | 1.6 | - | 41.1 | 1.3 | 2.4 | - |
| | 4 | 40.2 | - | 14.8 | 16.9 | 13.8 | - | - | - | 7.9 | 1.4 | 3.0 | - |
| | 5 | 73.4 | - | 3.0 | - | 10.1 | 1.0 | - | - | 10.7 | - | 0.7 | - |
| | 6 | 62.3 | - | 9.5 | 0.5 | 13.9 | 1.0 | - | - | 7.1 | 1.3 | 1.6 | - |
| | 7 | 64.3 | 0.8 | 7.4 | 2.6 | 10.0 | 0.6 | - | - | 5.7 | 2.2 | 1.9 | - |
| | 8 | 51.8 | - | 12.5 | - | 19.5 | 0.9 | - | - | 5.6 | 7.2 | 1.4 | - |
| | 9 | 67.5 | 0.6 | 3.9 | - | 12.4 | 0.9 | - | - | 12.2 | - | 0.7 | - |
| | 10 | 54.1 | - | 19.0 | 18.3 | - | - | - | 1.5 | - | - | - | - |

Table 4. Possible Phosphate Crystalline Phases [and Range in FOM] in the Scrubber Residue Fractions Based on XRPD[a]

| Element | Fraction | | | |
|---|---|---|---|---|
| | Untreated and Unleached | Untreated and Leached | Treated and Unleached | Treated and Leached |
| Ca | $Ca_5(P,Si,S)_3O_{12}(Cl,OH,F)$ [11.4-19.3]<br>$Ca_5(PO_4)_3OH$ [16.6-17.6]<br>$Ca_{10}(PO_4)_3(CO_3)(OH)_2$ [17.6-18.3]<br>$CaHPO_4$ [17.5-22.9] | — | $Ca_5(P,Si,S)_3O_{12}(Cl,OH,F)$ [17.6]<br>$\alpha$-$CaZn_2(PO_4)_2$ [13.6-14.0]<br>$Ca_{10}(PO_4)_3(CO_3)_3(OH)_2$ [14.1]<br>$CaFe_{12}(PO_4)_8(OH)_{12} \cdot 4H_2O$ [13.3-13.4] | $Ca_3Mg_2(PO_4)_4$ [19.2-19.6]<br>$Ca_3(PO_4)_2 \cdot xH_2O$ [14.4-16.6]<br>$\alpha$-$CaZn_2(PO_4)_2$ [12.7]<br>$Ca_5(P,Si,S)_3O_{12}(Cl,OH,F)$ [15.5] |
| Al | — | $Al_2(PO_4)(OH)_3$ [16.3-17.2] | $AlPO_4$ [20.7-21.3] | $AlPO_4$ [15.0-21.1]<br>$AlPO_4 \cdot xH_2O$ [11.0]<br>$Al_2(PO_4)(OH)_3 \cdot H_2O$ [15.0] |
| Na | $NaAl_3(PO_4)_2(OH)_4 \cdot 2H_2O$ [11.8-17.4] | — | — | $NaAl_3(PO_4)_2(OH)_4 \cdot 2H_2O$ [11.3-16.9]<br>$\chi$-$Na_3PO_4$ [16.8-21.0]<br>$NaCaPO_4$ [15.6-19.7]<br>$\alpha$-$NaMgPO_4$ [16.8-23.1] |
| Zn | — | — | $Zn_3(PO_4)_2 \cdot 2H_2O$ [17.5]<br>$ZnHPO_4 \cdot H_2O$ [14.5-16.1] | $Zn_3(PO_4)_2$ [22.6] |
| Fe | — | — | $Fe_5(PO_4)_3(OH)_5 \cdot H_2O$ [21.1]<br>$FePO_4 \cdot H_2O$ [15.5-17.4]<br>$FePO_4$ [18.2-19.3]<br>$(Fe,Mn)PO_4$ [17.1-18.9] | $Fe_5(PO_4)_4(OH)_2 \cdot 2H_2O$ [21.3]<br>$Fe_3(PO_4)_2(OH)_2$ [18.2] |
| K | — | — | $KPb_4(PO_4)_3$ [16.0-18.4]<br>$KPb_3(PO_4)_2(OH)_5 \cdot H_2O$ [13.2-16.4] | $KPb_4(PO_4)_3$ [11.7]<br>$KPb_3PO_4(SO_4)_2$ [17.1] |
| Mg | — | $(Mg,Fe)_3(PO_4)_2(OH)_{1.5} \cdot 1.5H_2O$ [14.3-22.6] | — | — |
| Cu | — | — | — | $CuFe_2(PO_4)_2(OH)_2$ [14.9-17.5]<br>$Cu_3(PO_4)(OH)_3$ [14.6-24.4] |
| Cd | $Cd_5(PO_4)_3Cl$ [11.0] | — | $Cd_3(PO_4)_2$ [17.9] | $Cd_5(PO_4)_3Cl$ [15.5]<br>$Cd_3(PO_4)_2$ [22.1] |

[a]Within any one element and fraction category, the possible mineral phases are listed vertically by decreasing likelihood of presence (based on average FOM).

Table 5. $^{31}P$ MAS NMR Data and Analysis

| Fraction | Component | $\delta_{iso}$ | $\delta_{11}$ | $\delta_{22}$ | $\delta_{33}$ | $\lvert\Delta\delta\rvert$ | % Comp | Probable Phases | Notes |
|---|---|---|---|---|---|---|---|---|---|
| Treated, Unleached | 1 | -0.30 | -27.3 | -1.5 | 27.9 | 42 | 45.8 | - | 2kHz[a] |
| | 2 | -1.43 | -57.1 | -9.8 | 62.6 | 96 | 54.2 | - | |
| | 1 | -0.67 | -36.5 | -6.8 | 41.2 | 63 | 60.1 | $CaHPO_4 \cdot 2H_2O$, $CaHPO_4$, $Ca_5(PO_4)_3OH$, $\alpha$-$CaZn_2(PO_4)_2$ | 4kHz[a] |
| | 2 | -0.98 | -104.4 | -18.4 | 119.9 | 181 | 39.9 | $Ca_2P_2O_7$ | |
| | 1 | -0.8 | -49.5 | -10.8 | 57.9 | 88 | 100 | - | 6kHz[a] |
| Treated, Leached | 1 | -0.95 | -62.1 | -2.3 | 61.6 | 94 | 72.9 | $CaHPO_4 \cdot 2H_2O$ | 6kHz[b] |
| | 2 | -9.16 | -55.5 | -55.4 | 83.5 | 139 | 27.1 | $Ca_2P_2O_7$ | |

[a]Spectra acquired with 10 μs, 90° $^{31}P$ pulse
[b]Spectra acquired with 4 μs, 90° $^{31}P$ pulse

Table 6. Possible Phosphate Mineral Phases in the Scrubber Residue Fractions Based on XPS

| Element | Fraction | | | |
|---|---|---|---|---|
| | Untreated and Unleached | Untreated and Leached | Treated and Unleached | Treated and Leached |
| Al[b] | (89,800 mg/Kg) | (178,700 mg/Kg) | (67,600 mg/Kg) | (106,500 mg/Kg) |
| | NA[c] | $AlPO_4$ | $AlPO_4$ | ND |
| Ca | (250,200 mg/Kg) | (42,700 mg/Kg) | (270,900 mg/Kg) | (135,100 mg/Kg) |
| | NA | $Ca_5(PO_4)_3OH$ | $Ca_5(PO_4)_3OH$ | $Ca(PO_4)_3OH$ |
| | | $Ca_5(PO_4)_3Cl$ | $Ca_5(PO_4)_3Cl$ | $Ca_5(PO_4)_3Cl$ |
| | | $\beta$-$Ca_3(PO_4)_2$ | $Ca_2P_2O_7$ | $Ca_2P_2O_7$ |
| | | | $Ca_8H_2(PO_4)_6 \cdot 5H_2O$ | $\beta$-$Ca_3(PO_4)_2$ |
| | | | $CaHPO_4$ | |
| Na | (57,700 mg/Kg) | (ND)[d] | (54,400 mg/Kg) | (ND) |
| | $Na_4P_2O_7$ | - | $Na_3PO_4$ | - |
| | | | $Na_4P_2O_7$ | |
| O | (239,300 mg/Kg) | (502,100 mg/Kg) | (309,600 mg/Kg) | (398,000 mg/Kg) |
| | $Na_4P_2O_7$ | NA | $Ca_5(PO_4)_3OH$ | $Ca_5(PO_4)_3OH$ |
| | | | $Ca_2P_2O_7$ | $Ca_5(PO_4)_3Cl$ |
| | | | $Na_4P_2O_7$ | $Ca_2P_2O_7$ |
| | | | | $Pb_5(PO_4)_3Cl$ |
| P | (ND) | (29,600 mg/Kg) | (34,900 mg/Kg) | (130,900 mg/Kg) |
| | NA | $AlPO_4$ | $AlPO_4$ | $Ca_5(PO_4)_3OH$ |
| | | $Ca_5(PO_4)_3OH$ | $Ca_5(PO_4)_3OH$ | $Ca_5(PO_4)_3Cl$ |
| | | $Ca_5(PO_4)_3Cl$ | $Ca_5(PO_4)_3Cl$ | $Ca_2P_2O_7$ |
| | | $\beta$-$Ca_3(PO_4)_2$ | $Ca_2P_2O_7$ | $\beta$-$Ca_3(PO_4)_2$ |
| | | $Pb_3(PO_4)_2$ | $Ca_8H_2(PO_4)_6 \cdot 5H_2O$ | $Pb_5(PO_4)_3Cl$ |
| | | | $CaHPO_4$ | |
| | | | $Na_3PO_4$ | |
| | | | $Na_4P_2O_7$ | |
| Pb | (16,000 mg/Kg) | 66,600 mg/Kg) | (ND) | 17,500 mg/Kg) |
| | NA | $Pb_3(PO_4)_2$ | - | $Pb_5(PO_4)_3Cl$ |

[a] Phases are listed alphabetically by first element.

[b] Surficial concentrations of the element in the indicated fraction are shown; concentrations based on XPS analysis and standard sensitivity factors.

[c] NA; no phosphate species assigned.

[d] ND; element not detected.

Table 7. Total Availability Leaching Data

| Constituent | Leachate Concentration, mg/L | | % of Available Fraction Stabilized Because of Treatment[a] |
|---|---|---|---|
| | Untreated | Treated | |
| Al | 5.0 | 1.1 | 75.5 |
| As | 0.030 | 0.028 | -3.8 |
| Ba | 2.0 | 1.3 | 27.7 |
| Ca | 1,540 | 1,290 | 6.8 |
| Cd | 0.600 | 0.337 | 37.5 |
| Cl | 522 | 433 | 7.7 |
| Cr | <0.04 | <0.04 | 0.0 |
| Cu | 0.66 | 0.25 | 57.9 |
| Fe | <0.04 | 0.26 | - |
| Hg | 0.0012 | 0.044 | -3,979 |
| K | 42 | 39 | - |
| Mg | 21.9 | 23.6 | -19.9 |
| Na | 51.5 | 46 | 0.6 |
| Pb | 2.3 | 0.01 | 99.5 |
| $PO_4^{3-}$ | 0.05 | 20.9 | -2,385 |
| Si | 40 | 71 | -97.5 |
| $SO_4^{3-}$ | 113 | 100 | 1.8 |
| Zn | 41.5 | 26.8 | 28.2 |
| Mass | - | - | 2.9 |

[a]Corrected for weight of $H_3PO_4$ added.

Table 8. Possible Controlling Solids and Their Saturation Indices

| Component | | | pH | | |
|---|---|---|---|---|---|
| | | | 4 | 6 | 8 |
| $Ca^{2+}$ | Ranked | $CaSO_4$ | 0.11 | -0.07 | -0.04 |
| | | $CaHPO_4$ | -0.03 | -0.04 | -0.49 |
| | | $CaSO_4 \cdot 2H_2O$ | 0.30 | 0.13 | 0.17 |
| | | $CaHPO_4 \cdot 2H_2O$ | -0.21 | -0.21 | -0.66 |
| | Other | $Ca_8H_2(PO_4)_6 \cdot 5H_2O$ | -28.07 | -10.38 | -4.60 |
| | | $\beta$-$Ca_3(PO_4)_2$ | -5.37 | 1.77 | 4.98 |
| | | $Ca_5(PO_4)_3OH$ | -15.09 | -2.48 | 4.26 |
| | | $Ca_5(PO_4)_3Cl$ | -10.81 | -0.31 | 4.41 |
| $Pb^{2+}$ | Ranked | $(Pb,Ca_4)(PO_4)_3Cl$ | 0.28 | 5.09 | 9.20 |
| | | $(Pb,Ca_4(PO_4)_3OH$ | -6.40 | 0.46 | 6.52 |
| | | $(Pb_2,Ca)(PO_4)_2$ | -3.74 | -0.84 | 0.95 |
| | | $(Pb,Ca_2)(PO_4)_2$ | -0.90 | 2.35 | 4.82 |
| | | $(Pb_3,Ca_2)(PO_4)_3OH$ | -8.12 | -1.62 | 3.77 |
| | Other | $Pb_5(PO_4)_3OH$ | -13.80 | -8.37 | -5.00 |
| | | $Pb_5(PO_4)_3Cl$ | 3.15 | 6.53 | 7.95 |
| | | $Pb_3(PO_4)_2$ | -6.72 | -4.19 | -3.06 |
| | | $PbHPO_4$ | -1.95 | -2.31 | -3.43 |

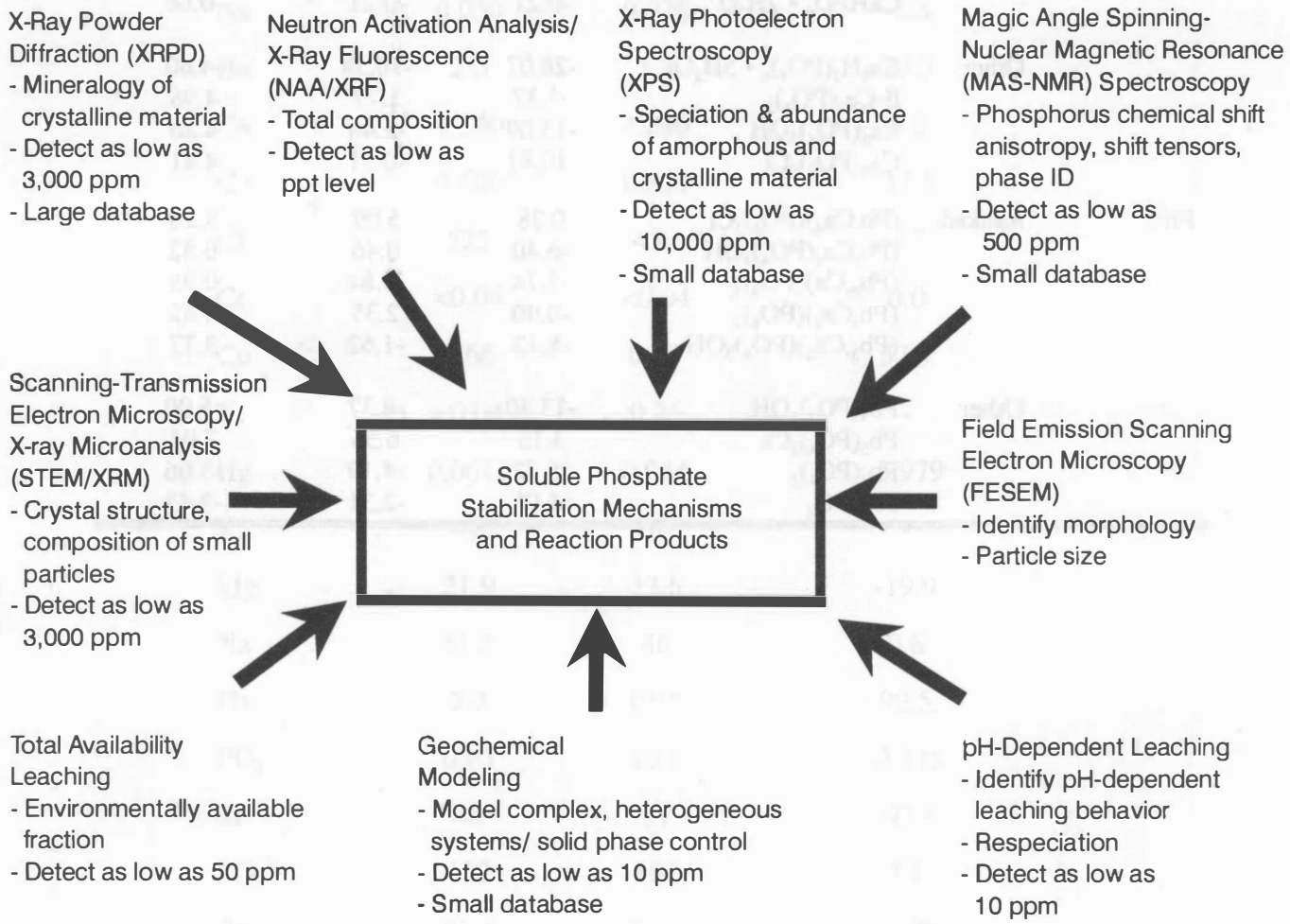


Figure 1. Schematic depicting approach used to identify stabilization reaction mechanisms and reaction products.

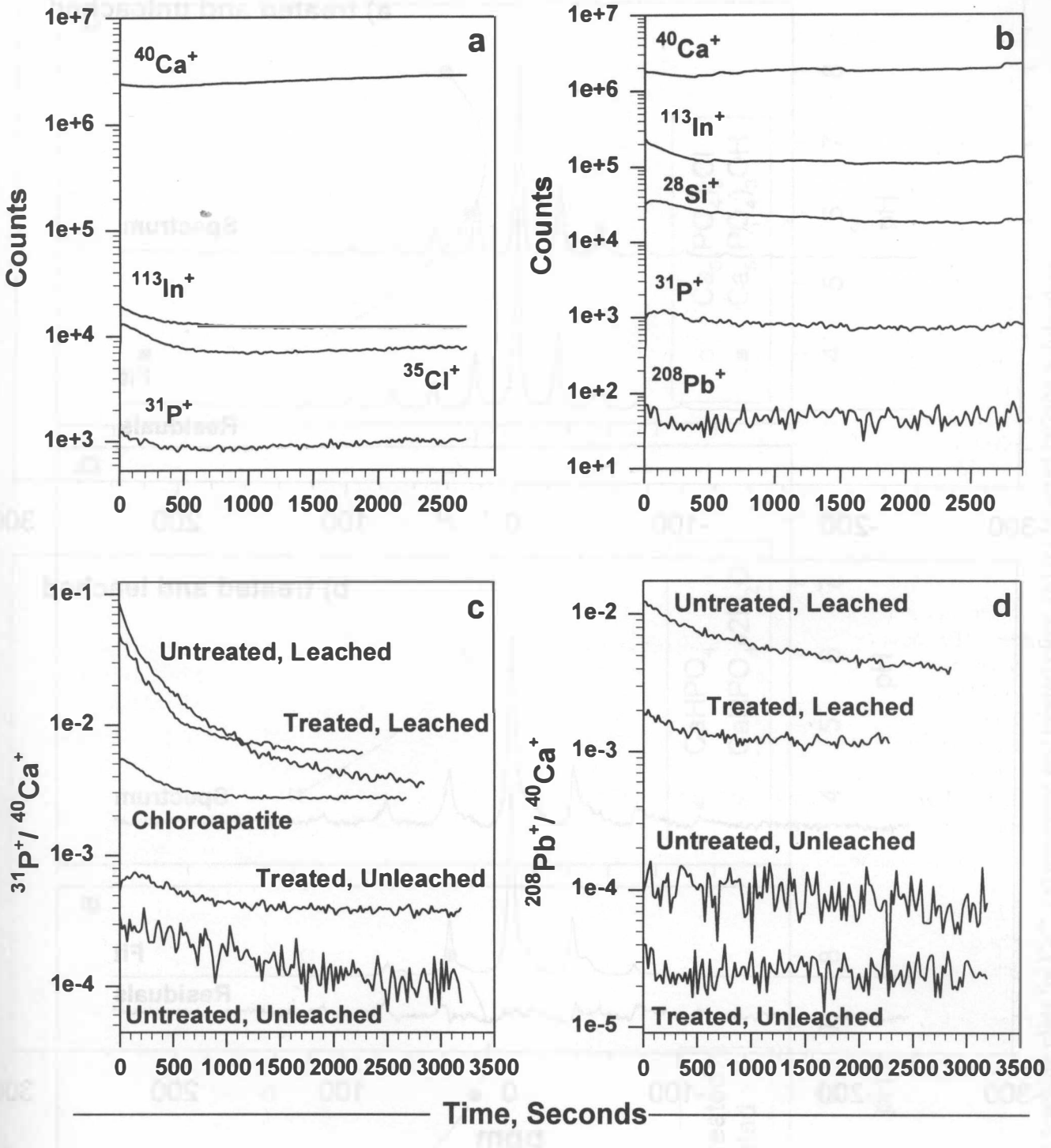


Figure 2. SIMS ion fragment depth profiles and ion fragment ratio depth profiles. (a) depth profiles for chloroapatite powder standard, (b) depth profiles for treated and leached fraction, (c) $^{31}P^+/^{40}Ca^+$ depth profiles, and (d) $^{208}Pb^+/^{40}Ca^+$ depth profiles.

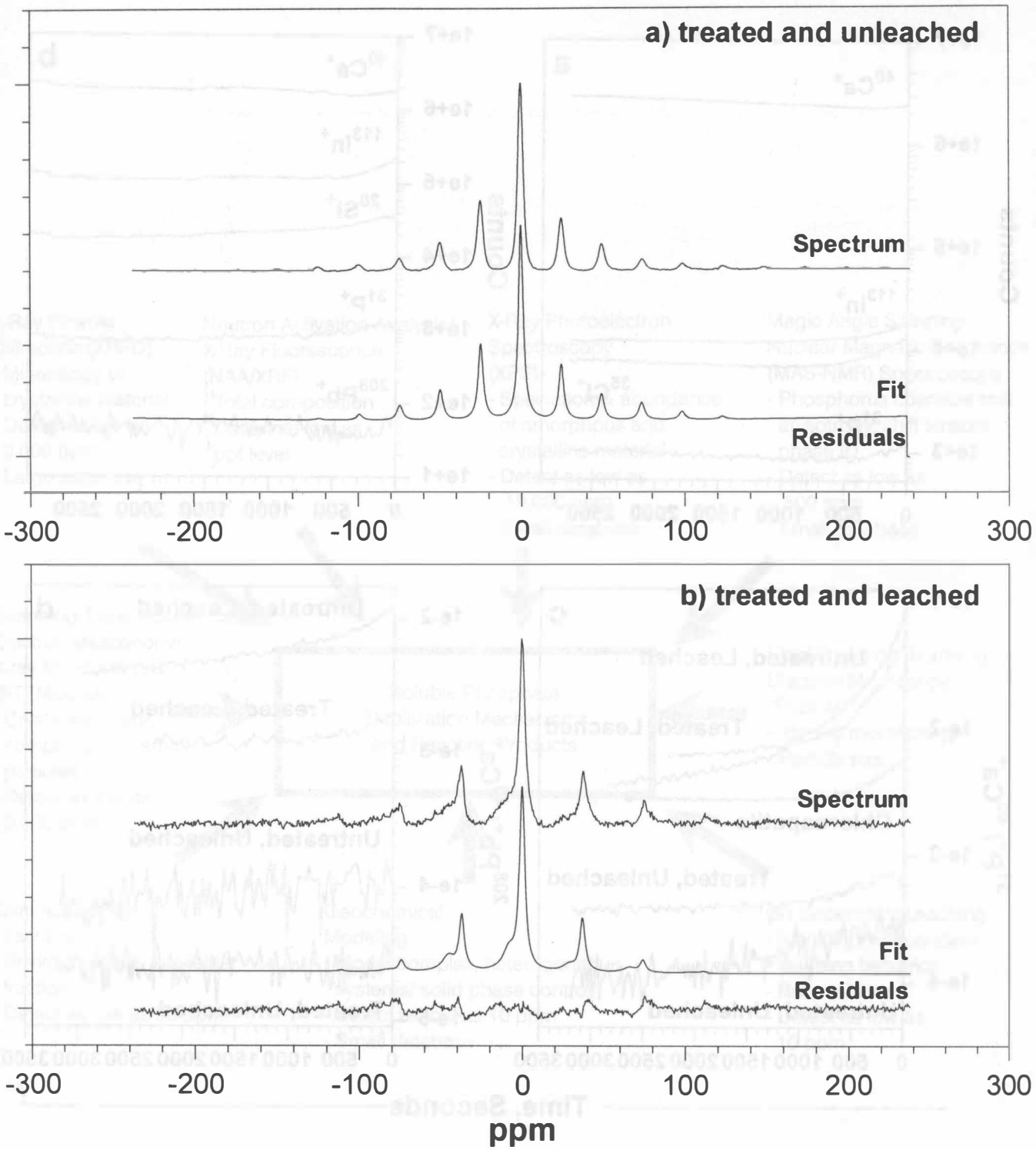


Figure 3. MAS-NMR spectra for (a) treated and unleached fraction and (b) treated and leached fraction.

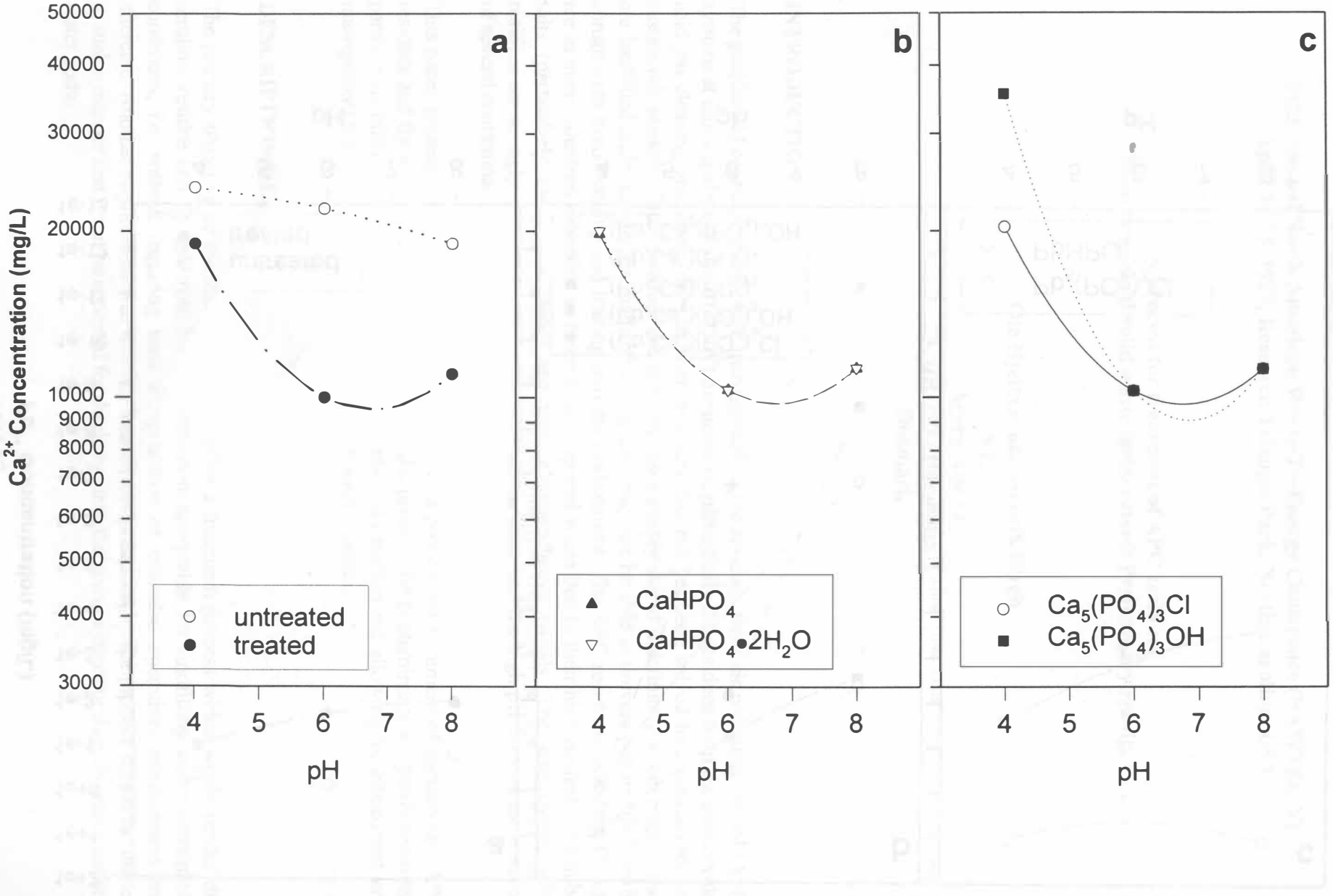


Figure 4. pH-dependent leaching plots for $Ca^{2+}$, (a) untreated and treated plots, (b),(c) selected infinite solids plots.

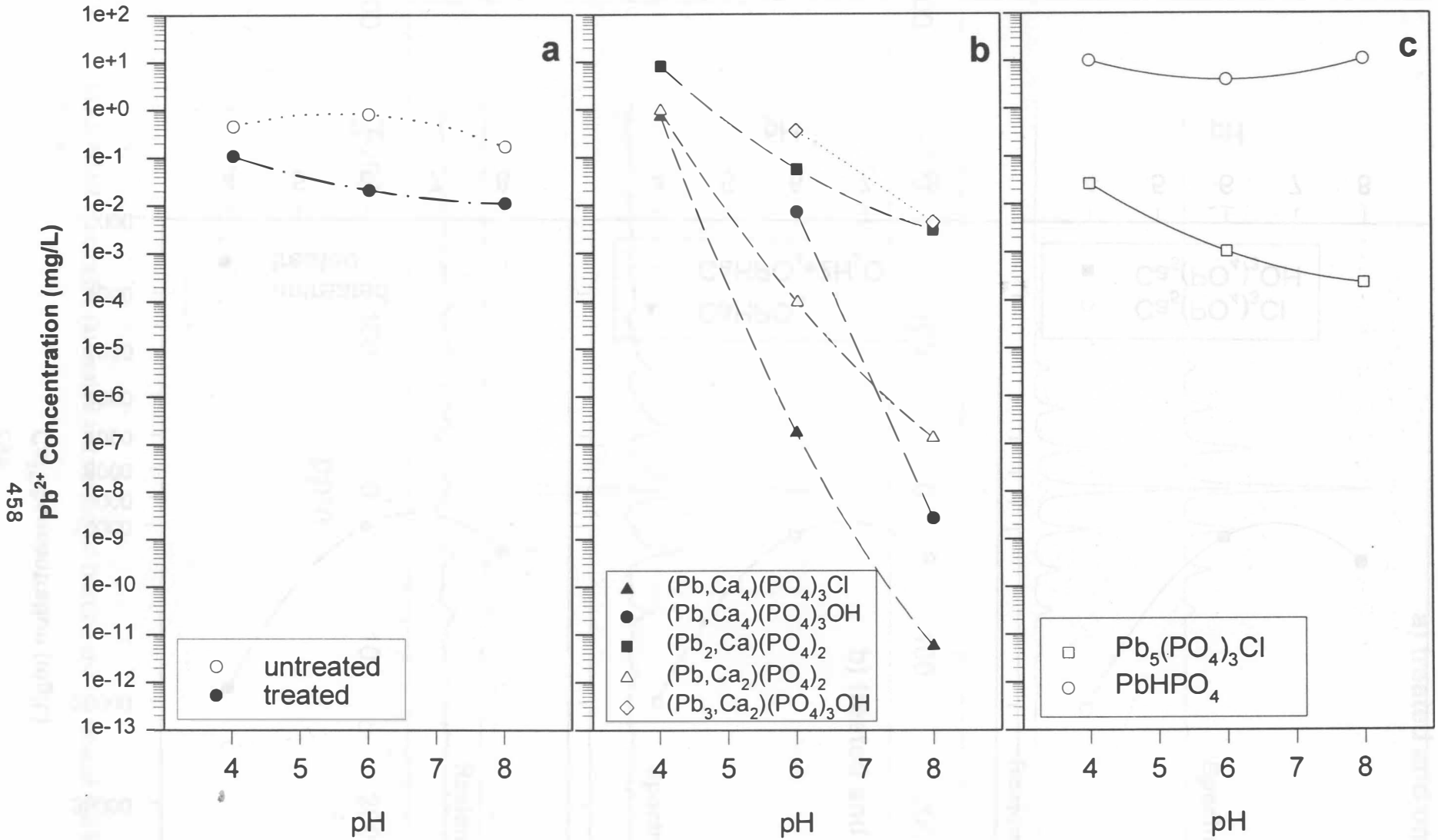


Figure 5. pH-dependent leaching plots for $Pb^{2+}$, (a) untreated and treated plots, (b),(c) selected infinite solids plot.